INTERNATIONAL JOURNAL OF HYDROGEN ENERGY 39 (2014) 10141–10153

Available online at www.sciencedirect.com

ScienceDirect

journal homepage: www.elsevier.com/locate/he

Catalytic CO_2 reforming of CH_4 over Cr-promoted Ni/char for H_2 production

Long Xu [a,b], *lin'e Duan* [b], *Mingchen Tang* [a], *Pei Liu* [b], *Xiaoxun Ma* [b], *Yulong Zhang* [c], *H. Gordon Harris* [a], *Maohong Fan* [a,d,*]

[a] *Department of Chemical and Petroleum Engineering, University of Wyoming, Laramie, WY 82071, USA*
[b] *Chemical Engineering Research Center of the Ministry of Education for Advanced Use Technology of Shanbei Energy, Shaanxi Research Center of Engineering Technology for Clean Coal Conversion, Northwest University of China, Xi'an 710069, PR China*
[c] *Western Research Institute, Laramie, WY 82072, USA*
[d] *School of Energy Resources, University of Wyoming, Laramie, WY 82071, USA*

ARTICLE INFO

Article history:
Received 28 February 2014
Received in revised form
20 April 2014
Accepted 22 April 2014
Available online 19 May 2014

Keywords:
CH_4–CO_2 reforming
Char
Ni
Cr
Nickel carbide

ABSTRACT

The objective of the study is to investigate the catalytic performance of Cr-promoted Ni/char in CO_2 reforming of CH_4 at 850 °C. The char obtained from the pyrolysis of a long-flame coal at 1000 °C was used as the support. The catalysts were prepared by incipient wetness impregnation methods with different metal precursor doping sequence. The characterization of the composite catalysts was evaluated by XRD, XPS, SEM-EDS, TEM, H_2-TPR, CO_2-TPD, CH_4-TPSR, and CO_2-TPO. The results indicate that the catalyst prepared by co-impregnation of Ni and Cr possess higher activity than those by sequential impregnation. The optimal loading of Cr on 5 wt% Ni/char is 7.8 wt‰. Moreover, the molar feed ratio of CH_4/CO_2 has a considerable effect on both the stability and the activity of Cr–Ni/char. The main effect of Cr is the great enhance of the adsorption to CO_2. It is interesting that the conversions of CH_4 and CO_2 over Cr-promoted Ni/char and Ni/char decrease initially, following by a steady rise as the reaction proceeds with time-on-stream (TOS). In addition, cyclic tests were conducted and no distinct deterioration in the catalytic performance of the catalysts was observed. On the basis of the obtained results, nickel carbide was speculated to be the active species which was formed during the CO_2 reforming of CH_4 reaction.

Introduction

CO_2 reforming of CH_4 or dry CH_4 reforming with several advantages [1–3], as shown in (R1),

$$CH_4 + CO_2 = 2CO + 2H_2 \quad \Delta H_{298} = 247.1\ \text{kJ/mol} \tag{R1}$$

has drawn increasing attention recently. This reaction converts two carbon-rich gases (CH_4 and CO_2) into synthesis gas (a combination of H_2 and CO). On one hand, both of the reactants

---

[*] *Corresponding author*. Department of Chemical and Petroleum Engineering, University of Wyoming, Laramie, WY 82071, USA. Tel.: +1 307 766 5633; fax: +1 307 766 6777.
E-mail address: mfan@uwyo.edu (M. Fan).

http://dx.doi.org/10.1016/j.ijhydene.2014.04.172

Table 1 – Proximate and ultimate analyses of Yulin coal and as-made coal char.

Sample	Proximate analysis (wt%, dry basis)			Ultimate analysis (wt%, dry basis)				
	A	V	FC	C	H	N	S	O*
Yulin coal	6.80	35.40	57.80	73.50	4.13	0.89	0.34	14.34
Yulin char	12.76	3.03	84.21	80.75	1.04	0.52	0.17	4.76

*: by diff.
A: ash; V: volatile matter; FC: fixed carbon.

are greenhouse gases and as such are intimately related to the impact of global warming impact [4,5]; their simultaneous utilization could mitigate depletion of other fossil fuels. On the other hand, this reaction can produce synthesis gas with a low H_2/CO ratio, which is favorable for the subsequent synthesis of long-chain hydrocarbons and other high value-added chemicals, especially via Fischer–Tropsch synthesis [1–3].

Due to the highly endothermic nature of this reforming reaction, elevated temperature is required for high conversions. In order to relieve this problem, efforts have been made to develop catalysts with high activity and stability. Group VIII transition metals have been widely reported for this application, among which, noble metal-based catalysts such as Rh, Ru, and Ir show higher activity and stability than Ni-based catalysts [6–9]. However, Ni-based catalysts are industrially preferred for their lower cost, although they are more sensitive to carbon deposition and sintering of Ni particles [10–12]. Apart from the metal, support plays a critical role. Al_2O_3 [13,14], SiO_2 [15], ZrO_2 [16], perovskite [17], and zeolites [18,19], were typically reported as good candidates for supporting materials. Coal char itself, as a cheap carbonaceous material, was reported as a promising catalyst for CO_2 reforming of CH_4 in recent studies [20–22]. Guo et al. found that char from coal with lower rank possessed better catalytic activity than that with higher rank [21]. However, the conversions of CH_4 and CO_2 catalyzed by char are much lower than those catalyzed by metal-based catalysts under similar reaction conditions, especially below 900 °C.

In this study, a novel catalyst was designed to take the advantages of both char and Ni-based catalysts as well as the introduction of Cr as the promoter. The influential factors such as impregnation sequences, Cr loadings, molar feed ratio of CH_4/CO_2, and the reusability of the catalyst were investigated. Finally, the reaction mechanism over the composite catalysts was proposed by the integration of catalytic performance and catalyst characterization which was realized by a variety of analytical techniques (XRD, XPS, SEM-EDS, TEM, H_2-TPR, CO_2-TPD, CH_4-TPSR, and CO_2-TPO).

Experimental

Catalyst preparation

The catalyst support was obtained from the pyrolysis of Yulin coal (a type of long-flame coal). The temperature was heated from ambient to 1000 °C at a heating rate of 10 °C/min, and kept isothermal for 1 h. The char was pre-sieved to 380–550 μm for further impregnation use. The proximate and ultimate analyses of Yulin coal and the as-made coal char are listed in Table 1.

The Ni/char catalyst was prepared by the incipient wetness impregnation method, in which the coal char was impregnated into an aqueous solution of $Ni(NO_3)_2$ with a predetermined Ni loading amount (5 wt% of the support). The Cr-modified Ni/char catalysts were prepared by either co-impregnation or sequential impregnation methods. The loadings of Ni and Cr were 5 wt% and 2.6 wt% of the char, respectively. In this case, $Ni(NO_3)_2 \cdot 6H_2O$ and $Cr(NO_3)_3 \cdot 9H_2O$ (Sigma–Aldrich, analytical grade) were used as active metal and promoter precursors, respectively. After the impregnation step, the sample was dried overnight at 110 °C. The catalysts prepared by co-impregnation, sequential impregnation (Cr before Ni), and sequential impregnation (Ni before Cr) are denoted as Cr&Ni/char, Ni∼Cr/char, Cr∼Ni/char, respectively. So as to investigate the effect of Cr loading on the catalytic performance, the loading of Cr on 5 wt% Ni/char was selected ranging from 5.2 wt‰ to 39.0 wt‰.

Catalyst characterization

The catalysts were subjected to characterization by XRD, XPS, SEM-EDS, TEM, H_2-TPR, CO_2-TPD, CH_4-TPSR, and CO_2-TPO. The X-ray powder diffraction (XRD) patterns of the catalysts were recorded by a Rigaku Smartlab X-ray diffractometer at a scanning rate of 4°/min in the 2θ scanning range of 20–80°. A Cu Kβ radiation source ($\lambda = 1.392$ Å) working at 40 kV and 40 mA was used in the tests. X-ray photoelectron spectroscopy (XPS) was measured with a Physical Electronics ESCA 5800 spectrometer which is equipped with a monochromatic Al Kα X-ray source ($E = 1486.6$ eV). The scanning step and working pressure were 0.1 eV and 2×10^{-9} mbar, respectively. Binding energies were calibrated to C 1s peak at 284.5 eV. The morphology and the particle size as well as the dispersion of the composite catalysts were studied by a scanning electron microscope along with an energy dispersive spectrometer (SEM-EDS, FEI, Quanta FEG MK2; Oxford Instruments America, Model #51-XMX0005) and a transmission electron microscopy (TEM, FEI, Tecnai G2 F20 S-Twin 200 kV). The particle size distribution was calculated by using Image J software.

Temperature-programmed reduction (TPR), temperature-programmed desorption (TPD), temperature-programmed surface reaction (TPSR), and temperature-programmed oxidation (TPO) were performed in a micro-reactor equipped with an on-line mass spectrometer (Hiden, HPR-20 QIC). A sample size of 150 mg was used for each run. For H_2-TPR, the catalyst was previously outgassed at 300 °C for 1 h under 20 ml/min He flow. As soon as the catalyst was cooled down to 50 °C, a 25 ml/min gas flow (10% H_2 in He) was introduced to the catalyst bed, then the temperature programming up to 800 °C with a heating rate of 10 °C/min was used for H_2-TPR test. For CO_2-TPD, the catalyst was pre-reduced with H_2 at 600 °C for 1 h and then outgassed at 300 °C for 1 h under He. As soon as the catalyst was cooled down to 50 °C, a 25 ml/min gas flow (10% CO_2 in He) was introduced to the catalyst bed for CO_2 adsorption. After CO_2 adsorption for 30 min, CO_2 flow was turned off while He flow was remained at 20 ml/min to sweep out the residue CO_2 from the entire process for another 30 min. Subsequently, the CO_2-TPD test was carried out by heating the catalysts to 800 °C with a heating rate of 10 °C/min. In the case of CH_4-TPSR test, the pre-reduced catalyst was heated to 950 °C at a heating rate of 10 °C/min under a 25 ml/min gas mixture (10% CH_4 in He). In order to determine the active species during reforming, the used catalysts, after the reforming reaction in the micro-reactor, were cooled down to 200 °C in He and also subjected to CH_4-TPSR. For CO_2-TPO experiments, the used catalyst was heated to 1050 °C with a ramp of 10 °C/min under 25 ml/min gas flow (10% CO_2 in He).

CO_2 reforming of CH_4

The CO_2 reforming of CH_4 experiments were carried out in a quartz fixed-bed reactor (3 mm ID) under atmospheric pressure, which was mounted inside a cylindrical and vertical electric furnace. The reactor temperature was measured by inserting a K-type thermocouple into the catalyst bed. Before the reaction, the system was purged with 30 ml/min of He for 30 min and the catalyst was then in situ reduced with constant H_2 flow (20 ml/min) at 600 °C for 1 h. All the reforming reactions were conducted at 850 °C. Various molar feed ratios of CH_4 to CO_2 (3:2, 1:1 and 2:3) with a total flow rate of 20 ml/min were investigated. The volumetric concentration of both the reactants and the products were monitored by means of an on-line gas chromatography (Shimazu GC-14C) installed with a thermal conductivity detector (TCD). After each reaction, He was introduced into the reactor bed again to purge gas out of the experimental apparatus and the reactor was cooled down to room temperature. The collected catalysts after reaction were subjected to characterization tests. The cyclic reforming experiments were carried out over 7.8 wt‰ Cr & 5 wt% Ni/char and 5 wt% Ni/char at 850 °C for 4 cycles, and each run last 8 h. As the preceding cyclic experiment ends, the

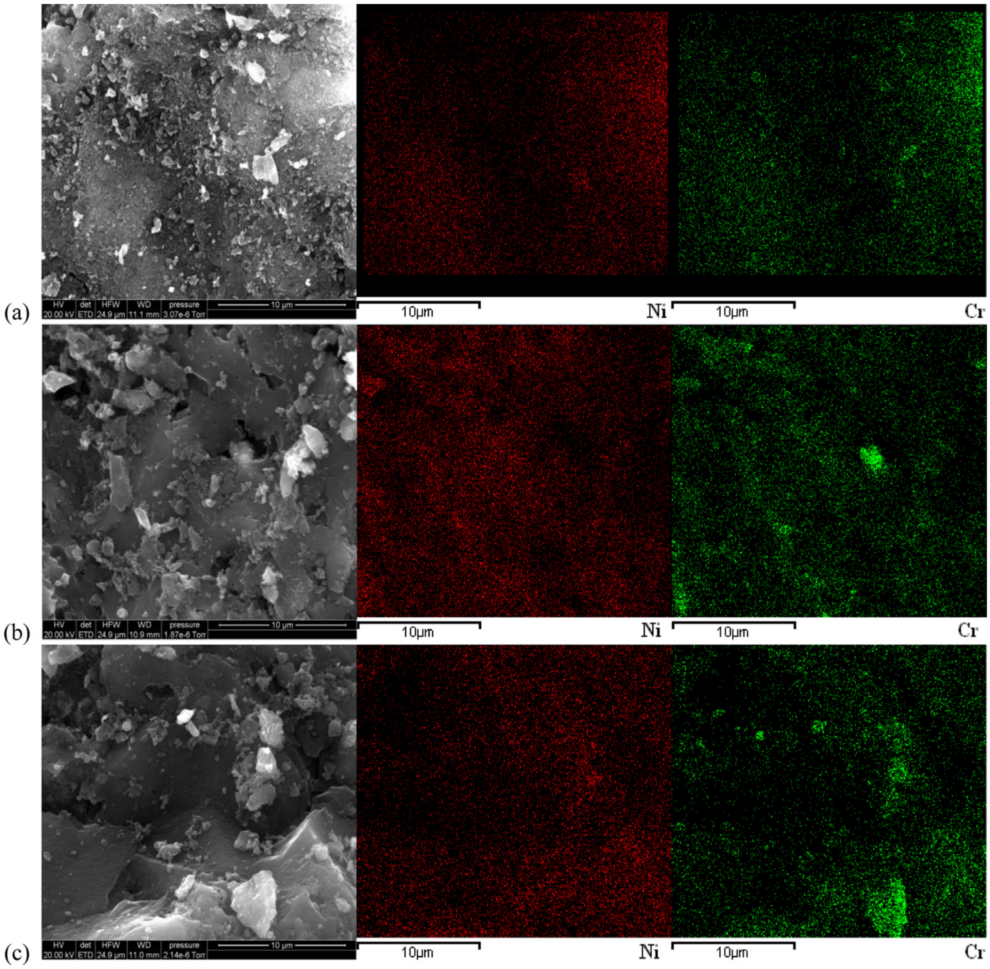

Fig. 1 – The SEM images of Cr-promoted Ni/char catalysts prepared by different impregnation sequences and the distribution of Ni and Cr on the catalyst surface. (a) Cr&Ni/char (co-impregnation); (b) Cr ~ Ni/char (sequential impregnation: first Ni then Cr); (c) Ni ~ Cr/char (sequential impregnation: first Cr then Ni). [Ni loading: 5 wt%; Cr loading: 2.6 wt%.]

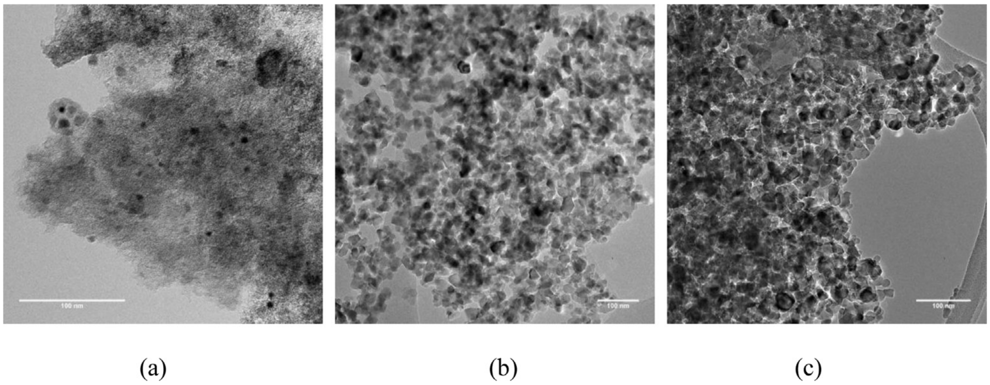

(a) (b) (c)

Fig. 2 – The TEM images of Cr-promoted Ni/char catalysts prepared by different impregnation sequences. (a) Cr&Ni/char (co-impregnation); (b) Cr~Ni/char (sequential impregnation: first Ni then Cr); (c) Ni~Cr/char (sequential impregnation: first Cr then Ni). [Ni loading: 5 wt%; Cr loading: 2.6 wt%.]

used catalyst was cooled down rapidly by exposing the catalyst directly to the ambient and left for 12 h. It is noteworthy that no further activation treatment for catalyst was employed before the catalyst was used for the next cycle. The conversions of CH_4 and CO_2 were calculated as follows:

$$CH_4 \text{ conversion, } \% = 100 \times \frac{(CH_{4,in} - CH_{4,out})}{CH_{4,in}} \tag{E1}$$

$$CO_2 \text{ conversion, } \% = 100 \times \frac{(CO_{2,in} - CO_{2,out})}{CO_{2,in}} \tag{E2}$$

where $CH_{4,in}$, $CO_{2,in}$ and $CH_{4,out}$, $CO_{2,out}$ represent the molar flow rate of each gas component at the inlet and outlet of the reactor, respectively.

Results and discussion

Effect of impregnation sequence

Fig. 1 shows the SEM images of Cr-promoted Ni/char catalysts prepared by different impregnation sequences and the distribution of Ni and Cr on the catalyst surface.

Unlike well-ordered supporting materials, char generally possesses tough and irregular morphology on the surface. Among the catalysts prepared via three different impregnation sequences, the most even dispersion of both Ni and Cr can be observed on the surface of Cr&Ni/char catalyst. Complementally, the atomic ratios of Ni/Cr calculated from the EDS results in terms of Cr&Ni/char, Cr~Ni/char, and Ni~Cr/char are 1.43, 2.96, and 1.29, respectively. The difference among the Ni/Cr ratios over the composite catalysts might lie in the different sorption ability of Ni^{2+} and Cr^{3+} onto the activated carbon support. In the case of co-impregnation for Cr&Ni/char, the binding sites of the support could be competitively divided upon simultaneous addition of the binary metal ions. While in the case of sequential impregnations for Cr~Ni/char and Ni~Cr/char, the preceding impregnated metal ion which is bonded with the support could entirely change the surface properties of support thereby has a significant impact on the addition of second metal ion. Makeswari et al. [23] studied the competitive sorption between Ni^{2+} and Cr^{3+} onto activated carbon and found that the electronegativity of metal ion is a dominant factor for competitive sorption; since the electronegativity of Ni^{2+} (1.75, Pauling scale) is more than that of Cr^{3+} (1.66, Pauling scale), Cr^{3+} in the binary solution weakly affects Ni^{2+} uptake on the activated carbon. According to this explanation, Ni^{2+} would have stronger affinity with the support than Cr^{3+}, hence, Cr&Ni/char and Ni~Cr/char possesses similar Ni/Cr ratios; whereas, the difference between Cr&Ni/char and Cr~Ni/char is remarkable.

The TEM images of Cr-promoted Ni/char catalysts prepared by different impregnation sequences are presented in Fig. 2, among which the most highly dispersed Ni particles can be observed on the surface of Cr&Ni/char catalyst. The mean Ni particle sizes on the surface of Cr&Ni/char, Cr~Ni/char, and Ni~Cr/char catalysts were calculated as 9.3 nm, 23.2 nm, and 18.4 nm, respectively. Therefore, the impregnation sequence is demonstrated to have a significantly impact on the dispersion of Ni particles. Comparably, the co-impregnation could achieve better Ni dispersion than the sequential impregnation. The uneven Ni dispersion and larger particle size as a consequence of sequential impregnation could have a negative effect on the catalytic performance which will be discussed later.

Fig. 3 shows the influence of different impregnation sequences on catalytic performance. The variations in both CH_4 and CO_2 conversions with TOS at 850 °C over the catalysts prepared by three different impregnation sequences are presented in Fig. 3(a); the changes in the H_2/CO ratios are also given in Fig. 3(b). Among the three composite catalysts, Cr~Ni/char and Ni~Cr/char exhibit similar activity with respect to the reactant conversions under the given reaction conditions, while Cr&Ni/char shows higher CH_4 and CO_2 conversions than the other two catalysts by approximately 9% and 7% (absolute value), respectively. Besides, the H_2/CO ratios over Cr&Ni/char, Cr~Ni/char and Ni~Cr/char tend to be stable above 180 °C and retain respectively at the values of 0.899, 0.877, and 0.861 after 20 min TOS. Oezkara-Aydinoglu et al. [24] investigated the impregnation strategy on the

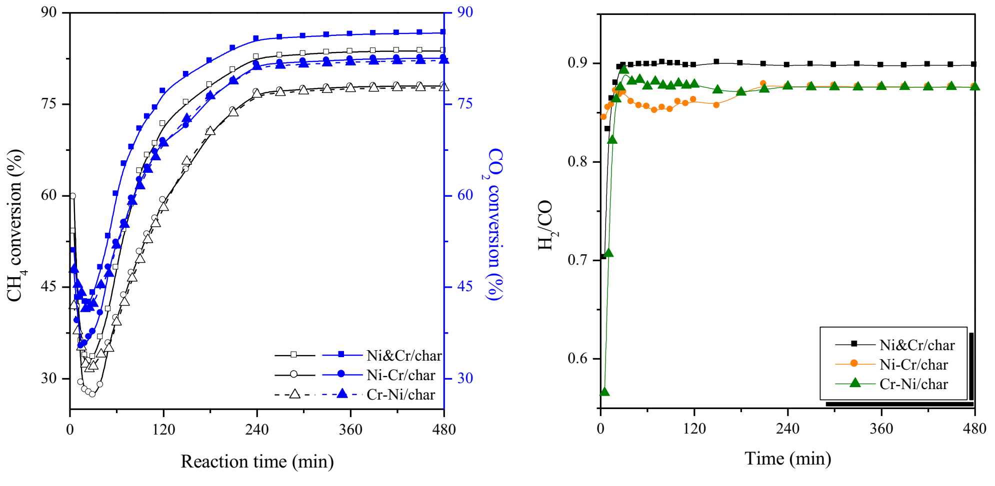

(a) (b)

Fig. 3 – Effect of impregnation sequence on catalytic performance. (a) The conversions of CH_4 and CO_2; (b) The molar ratio of H_2/CO. [Temperature: 850 °C; Feed flow rate: 20 ml/min; $CH_4/CO_2 = 1$; Ni loading: 5 wt%; Cr loading: 2.6 wt%.]

activity and stability of 1 wt%Ce–1 wt%Pt/ZrO_2 catalyst in CO_2 reforming of CH_4 and found that the catalyst prepared by co-impregnation has stronger surface interaction between Pt and Ce resulting in better catalytic activity than that by sequential impregnation. Koo et al. [25] reported 12 wt% Ni–6 wt%Ce/Al_2O_3 catalysts prepared by co-impregnation exhibits higher catalytic performance and less coke formation than those prepared by sequential impregnation in a combined steam and CO_2 reforming of CH_4 reaction due to an enhancement in Ni dispersion. Moreover, Yoshida et al. [26] found that the bimetallic (Pd and Ni) catalysts prepared by the co-impregnation method show higher resistance to hot-spot formation than those prepared by sequential impregnation in oxidative steam reforming of CH_4 partly because of the decrease of average metal particle size. However, the influence mechanism regarding impregnation sequence is complex, and various factors such that the type of metal, the amount of metal, and the interaction between metal and support could have impacts in varying degrees [25–28]. Through the results of catalytic performance, a preliminary conclusion could be drawn here that the Cr-promoted Ni/char catalysts prepared by the co-impregnation has higher activity than the others prepared by sequential impregnation in this research.

According to Fig. 3, it is also observed that the conversions of both CH_4 and CO_2 initially decrease within 20 min TOS, following by a progressive rise to the steady levels eventually, which are much higher than the initial ones. The interesting phenomenon will be discussed later on. Meanwhile, on the basis of foregoing results regarding the effect of impregnation sequence Cr&Ni/char was screened out to be employed on more in-depth study of this interesting observation.

Effect of Cr loading

The conversions of CH_4 and CO_2 as well as the molar ratios of H_2/CO over 5 wt% Ni/char catalysts with various Cr contents at 850 °C are shown in Fig. 4. Obviously, both CH_4 and CO_2 conversions reach a maximum and then decrease with increasing Cr contents; in another word, there is an optimal loading for Cr. It can also be noted that all the catalysts with Cr content ranging from 0 to 26 wt‰ have a H_2/CO ratio which remains unchanged at about 0.9. However, a decrease in the H_2/CO ratio occurs when Cr content is as high as 39 wt‰. Moreover, the catalysts with Cr loadings ranging from 7.8 wt‰ to 13.0 wt‰ show similar conversions, which are higher than the other Cr loadings under the same experimental conditions. Hence, 7.8 wt‰ would be the best choice for Cr loading. Hereafter, the catalyst denoted as 7.8 wt‰ Cr & 5 wt% Ni/char will be focused on for further investigation of the catalytic behavior. Nagaoka et al. studied the effect of Cr on $Co_{0.054}Ni_{0.018}Mg_{0.93}O$ solid solution for $CH_4/CO_2/H_2O$ reforming and proposed that the dispersion of nickel species could be enhanced by limited and lower Cr loadings; they also concluded that Cr acts as a glue for sticking the support materials to each other and thereby induces the aggregation of the metal particles with the presence of excess Cr [29]. Apart from the optimum Cr loading, an unusual variation trend was detected. The initial CH_4 and CO_2 conversions over 7.8 wt‰ Cr & 5 wt% Ni/char after 5 min TOS are 56.8% and 48.8%, respectively. The conversions then shortly reach their minimums (33.0% for CH_4 and 43.9% for CO_2) after 15 min TOS. Subsequently, the conversions start to rise and almost double the initial ones after 45 min TOS. Both CH_4 and CO_2 conversions reach above 90% after 2 h TOS and negligible increase in the conversions could be observed afterward.

Effect of the molar feed ratio of CH_4/CO_2 on the catalytic activity over 7.8 wt‰ Cr & 5 wt% Ni/char

The effect of molar feed ratio of CH_4/CO_2 on the CH_4 and CO_2 conversions as well as of the H_2/CO ratio over 7.8 wt‰ Cr & 5 wt% Ni/char at 850 °C is illustrated in Fig. 5. The initial conversions of CH_4 with the molar feed ratios of CH_4/CO_2 (2:3,

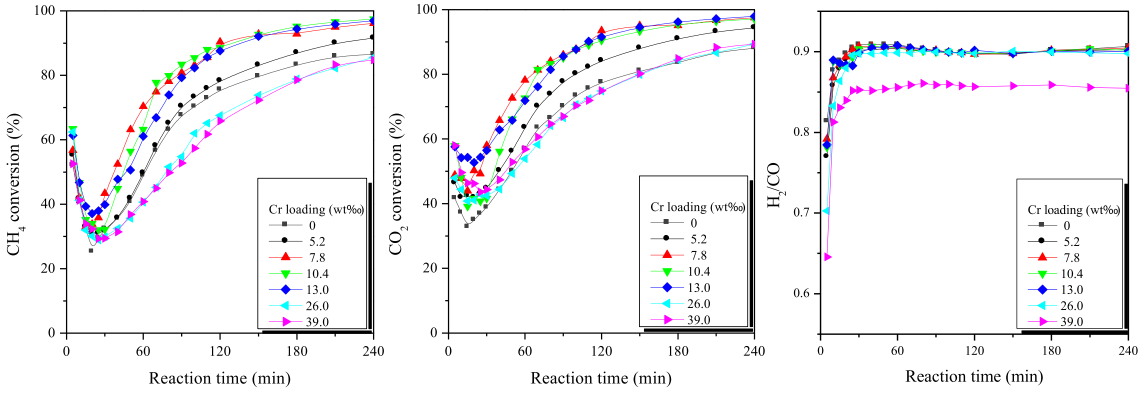

(a) (b) (c)

Fig. 4 – Effect of Cr loading over Ni/char on catalytic performance. (a) The conversion CH_4; (b) The conversion of CO_2; (c) The molar ratio of H_2/CO. [Temperature: 850 °C; Feed flow rate: 20 ml/min; $CH_4/CO_2 = 1$; Ni loading: 5 wt%.]

1:1, and 3:2) are 61.6%, 56.8%, and 28.3% after 5 min TOS, respectively. The initial CH_4 conversions decrease as the CH_4 concentration increases in the feed. When the molar feed ratio of CH_4/CO_2 was set at 2:3 and 1:1, the CH_4 conversions have a slight decrease within the initial 15 min TOS and rise afterward; whereas no decline in the CH_4 conversion could be observed initially when the CH_4/CO_2 ratio was set at 3:2, and the CH_4 conversion keeps rising until it reaches about 80% after 1 h TOS. In the case of CO_2 conversion, it decreases as CO_2 concentration increases in the feed throughout the entire experimental time range. For the CH_4/CO_2 ratio equal or less than unity, the CO_2 conversion decreases at first and then increases; whereas, the CO_2 conversion keeps rising until it reaches about 100% after 1 h TOS when the CH_4/CO_2 in the feed exceeds unity. According to the characteristic of CO_2 reforming of CH_4 reaction, a CH_4/CO_2 feed ratio close to unity is required to achieve higher conversions. In addition, it seems that the trend of conversion is interrelated with the feed ratio of CH_4/CO_2, or the decrease of conversion within 20 min TOS would disappear with the increasing CH_4 concentration in the feed. As depicted from Fig. 4(b), the ratios of H_2/CO are stable at 0.75, 0.90, and 1.13 with an increase of CH_4 concentration in the feed, indicating that higher CH_4/CO_2 ratios in the feed would lead to higher ratios of H_2/CO in the products. The results reveal that it is important to control the H_2/CO ratio of syngas product by adjusting the CH_4/CO_2 ratio in the feed.

Fig. 6 shows the SEM images of 7.8 wt‰ Cr & 5 wt% Ni/char catalyst prior to and after reforming reaction with different feed ratios. According to Fig. 6, the agglomeration of the active phase becomes severe after reaction with the molar feed ratio

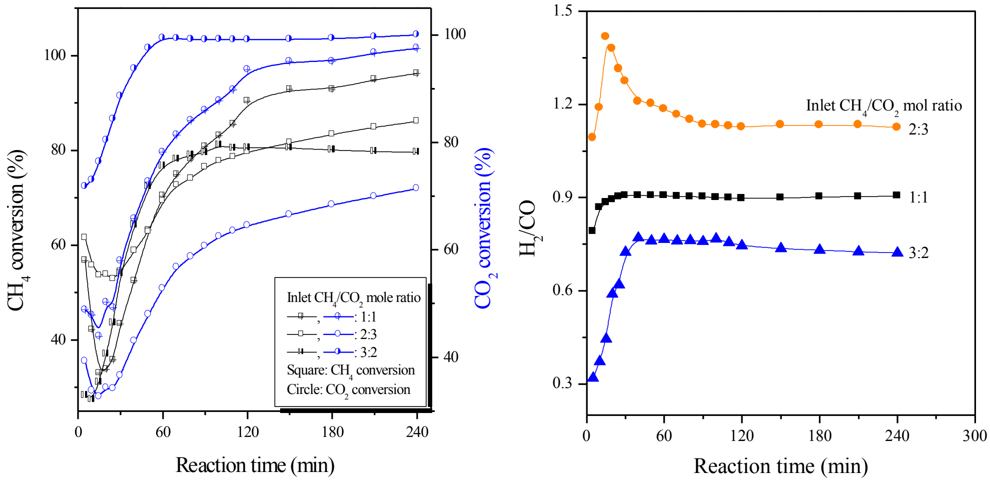

(a) (b)

Fig. 5 – Effect of the molar feed ratio of CH_4/CO_2 on catalytic performance over 7.8 wt‰ Cr & 5 wt% Ni/char. (a) The conversions of CH_4 and CO_2; (b) The molar ratio of H_2/CO. [Temperature: 850 °C; Feed flow rate: 20 ml/min; Ni loading: 5 wt%; Cr loading: 7.8 wt‰.]

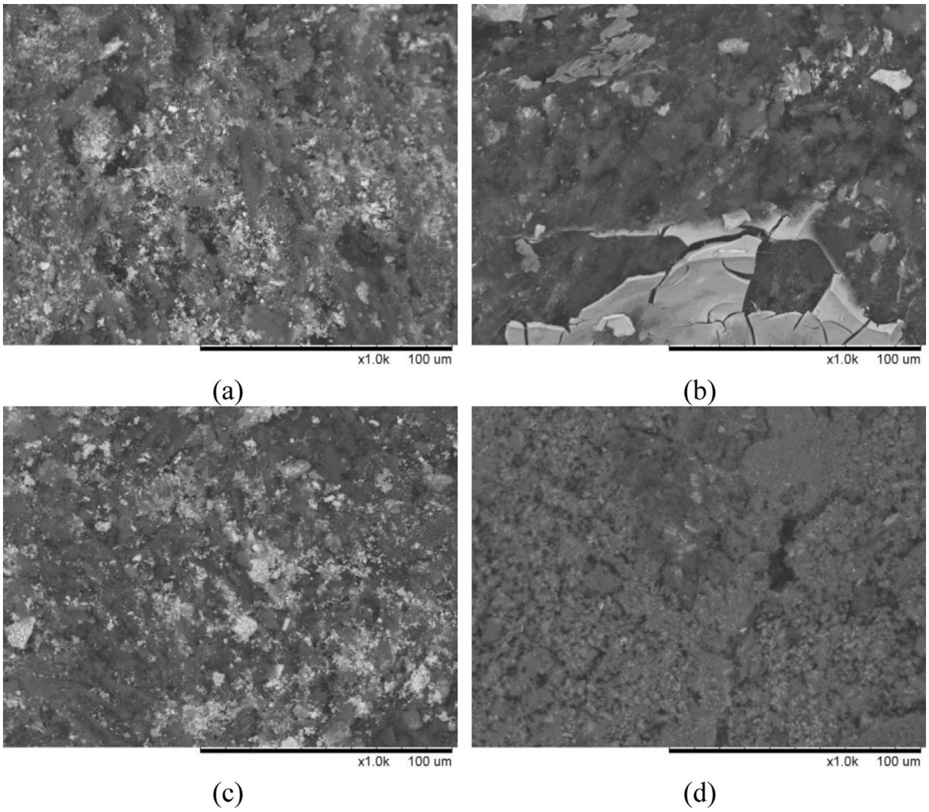

(a) (b)

(c) (d)

Fig. 6 – The SEM images of the fresh Cr&Ni/char and the used ones reforming in different feed ratio of CH_4/CO_2. (a) Fresh Cr&Ni/char; (b) Used Cr&Ni/char in $CH_4/CO_2 = 2:3$; (c) Used Cr&Ni/char in $CH_4/CO_2 = 1:1$; (d) Used Cr&Ni/char in $CH_4/CO_2 = 3:2$. [Reaction temperature: 850 °C; Reaction time: 8 h; Feed flow rate: 20 ml/min; Ni loading: 5 wt%; Cr loading: 7.8 wt‱.]

of CH_4/CO_2 equal to 2:3, while there are no significant changes on the catalyst surface with the molar feed ratio of CH_4/CO_2 equal to 1:1. The surface of the catalyst is dim after reaction with the molar feed ratio of CH_4/CO_2 equal to 3:2, being attributed to the shielding of carbon deposition originating from CH_4 dissociation.

The reusability of 7.8 wt‱ Cr & 5 wt% Ni/char

The catalytic performance of 5 wt% Ni/char and 7.8 wt‱ Cr & 5 wt% Ni/char during four cycles at 850 °C is illustrated in Fig. 7. As depicted from Fig. 7, both catalysts exhibit similar variation tendencies as time proceeds during all the cycles. It is also noted that the CH_4 and CO_2 conversions over Cr-promoted Ni/char are always roughly 10% (absolute value) higher than those over the catalyst without Cr promotion throughout the entire TOS range. The initial conversions of CH_4 and CO_2 during cycles 2, 3 and 4 are observed to be much higher than those during cycle 1. In addition, it takes less time for both reactant conversions to reach steady state during cycles 2, 3, and 4 than cycle 1. For instance, in the case of Cr-promoted Ni/char catalyst during the 1st cycle, it takes about 120 min for CH_4 and CO_2 conversions to reach 90%; whereas it takes only 50 min for cycle 2 to reach the same conversions of CH_4 and CO_2. Negligible difference could be detected for cycle

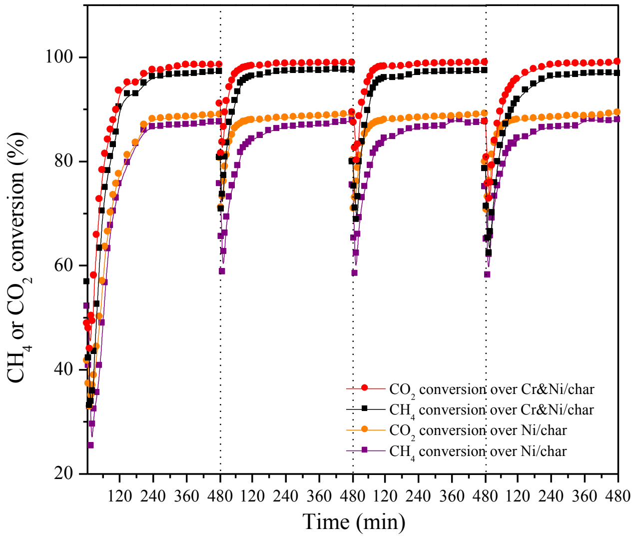

Fig. 7 – The catalytic performance of Ni/char and Cr&Ni/char in cyclic experiments. [Reaction temperature: 850 °C; Feed flow rate: 20 ml/min; $CH_4/CO_2 = 1$; Ni loading: 5 wt%; Cr loading: 7.8 wt‱.]

2 and cycle 3 with respect to the conversions of CH_4 and CO_2. Furthermore, the H_2/CO ratios do not differ too much from each other and remain almost constant at the value of 0.9. Therefore, without additional treatment, both Ni/char catalysts with and without Cr addition have unique stability and promising activity during consecutive cyclic reforming reactions.

Mechanism

On the basis of foregoing results, one might wonder why there are inflection points for the conversions of CH_4 and CO_2 at about 15 min with the molar feed ratio of CH_4/CO_2 equal or less than 1; and questions regarding the disappearance of inflection points in conversions as the concentration of CH_4 increases.

The bulk phases of the char-based catalysts in three stages (fresh, reduced, and used) were determined by XRD as presented in Fig. 8. The strong peak at 26.2° is ascribed to the diffraction of C (0 0 2) of turbostratic carbon [30]. The peaks at 37.5°, 43.4° and 63.0° are attributed to NiO crystalline phase [10,11]. For catalysts in the fresh stage, NiO peaks are too weak to be used to calculate the crystallite sizes of NiO with the Scherrer equation. Such weak peaks of NiO in the XRD patterns indicate that the NiO particles were well-dispersed on the char. The peaks at 44.4°, 51.8° and 76.4° are due to metallic Ni phase [31,32]. For the catalyst without addition of Cr after H_2 reduction, the remarkable peaks at 44.4°, 51.8° and 76.4° appear, suggesting the reduction of NiO to Ni under such pretreatment; the Ni particle size is 157 Å calculated by Scherrer equation. For the Cr-promoted catalyst after reduction, the peak signals of Ni are comparably weaker, indicating smaller Ni particles formation by the enhancement of Cr addition. For used catalyst, distinct diffraction peaks of Ni were detected, suggesting the growth of Ni particles during the reaction. The Ni particle sizes over Ni/char and Cr&Ni/char are 641 Å and 438 Å, respectively, indicating that the addition of Cr could improve the dispersion of Ni and lead to smaller Ni particles. However, Cr itself does not reflect on the XRD patterns since such a small quantity of Ce loading is below the detection limit of XRD. It is widely accepted that the dramatic increase in the crystallite size of Ni particle is responsible for the loss in catalyst activity during reaction [33]. As the reaction proceeds, the size of Ni crystal particle could increase and the persistent growth of deposited carbon on the catalyst surface would block the active sites, causing an irreversible deactivation of catalyst. Typically, this drastic drop in catalyst activity could be observed at the beginning of reaction.

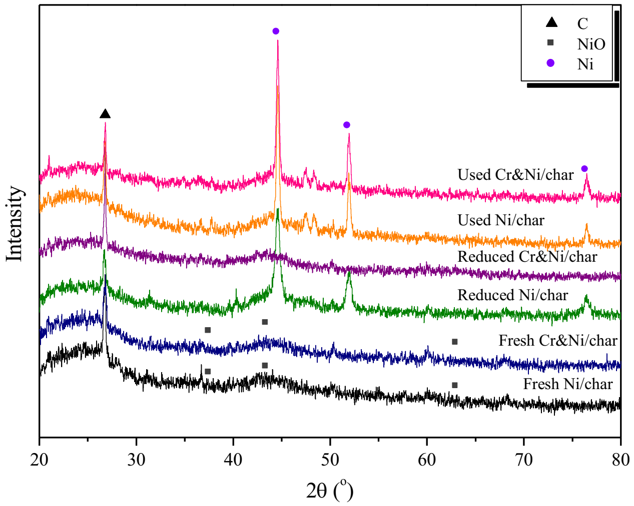

Fig. 8 – The XRD patterns of Ni/char and Cr&Ni/char. [Reduced conditions: 600 °C, 20 ml/min H_2, 1 h; Reaction conditions: 850 °C, 8 h, Feed flow rate of 20 ml/min, $CH_4/CO_2 = 1$; Ni loading: 5 wt%; Cr loading: 7.8 wt‰.]

Even though Ni alone can be considered as the active species during the reforming reaction, the experimental results could not support this simplex viewpoint and discussion in terms of another active species will be given as follow. As mentioned earlier, the existence of the inflection points for CH_4 and CO_2 conversions might be intimately related to the carbon formation, where two possibilities could be speculated here: (i) the diffraction peaks of the potential active species are difficult to be identified due to peak overlapping with the other distinct components; (ii) the particle size of the new active species is too small to exhibit a distinct signal on the XRD patterns. It is therefore conjectured that Ni_3C might be the key to answer the argument proposed. Goto et al. reported that the diffraction peaks of Ni_3C have characteristic theta angles which are close to those of Ni; thereby it is difficult to isolate these two species by traditional XRD detection method [34]. Hence, XPS technique was employed to make up the deficiency of XRD in the application of Ni_3C detection.

Fig. 9 shows the XPS spectra in the C1s region of the raw support (char), the used Ni/char, and the used Cr&Ni/char. According to Fig. 9, the remarkable change in C1s spectra among the support and the used catalysts is the obvious peak broadening of C1s after reaction, suggesting the appearance of another carbon species. According to the position data of binding energy from NIST X-ray Photoelectron Spectroscopy Database (NIST Standard Reference Database 20, Version 4.1), the C1s spectra could be resolved into various types of carbon species (3 for char support, 4 for the used catalysts). The binding energies centered at 283.9, 284.5, 285.5, and 286.4 eV are attributed to Ni_3C, C=C, C–C, and C–O, respectively. The latter three carbon species correspond to the inherent structures of char, while Ni_3C specie is unique and could not be found on the char support naturally. Moreover, the amount of this carbide material, Ni_3C, on the surface of used 7.8 wt‰ Cr & 5 wt% Ni/char and 5 wt% Ni/char constitutes approximately 15% and 10% of the total carbon content, respectively. Kroll et al. noticed a similar change of C1s spectra by XPS during the investigation of the active phase over Ni/SiO_2 catalyst in CH_4–CO_2 reforming; by using techniques including XPS, steady-state isotopic transient kinetics analysis, and magnetic measurement, they concluded that nickel carbide-like layers, established in the initial period of the run, constitute the active phase for the reaction with little dependence on the particle morphology and the degree of nickel reduction [35].

The XPS spectra in the Ni 2p region of the reduced Ni/char, the used Ni/char, and the used Cr&Ni/char are also presented in Fig. 10. For the reduced Ni/char, the binding energies positioned at 852.4 eV and 870.0 eV could be attributed to 2p 3/2 and 2p 1/2 of metallic Ni, respectively; meanwhile, the binding

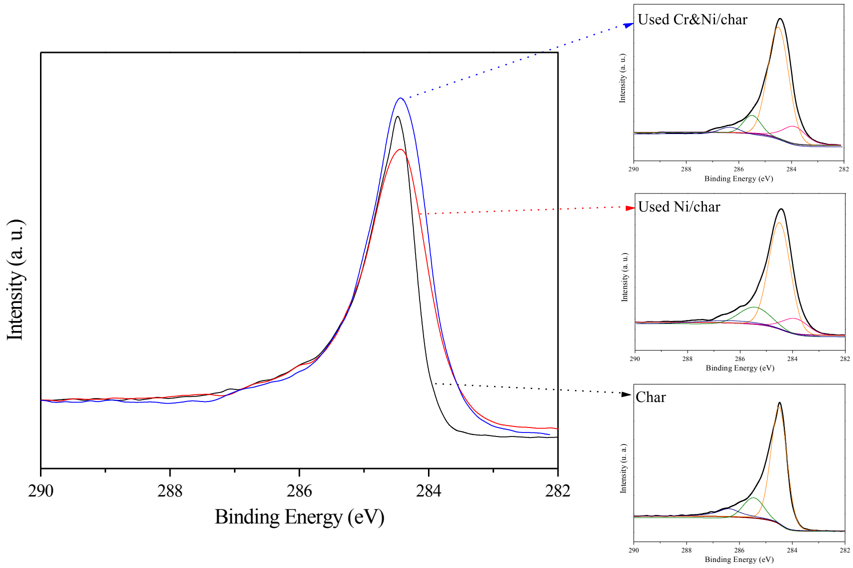

Fig. 9 – **The XPS spectra in the C1s region of the raw support (char), the used Ni/char, and the used Cr&Ni/char. [Reaction conditions: 850 °C, 8 h, Feed flow rate of 20 ml/min, $CH_4/CO_2 = 1$; Ni loading: 5 wt%; Cr loading: 7.8 wt‰.]**

energies at 857.7 eV and 876.2 eV could be ascribed as the Ni satellites of 2p 3/2 and 2p 1/2. For the used catalysts, a remarkable shift of Ni 2p 3/2 (0.6 eV) to higher binding energy (853.0 eV) and the appearance of more satellite peaks are observed, suggesting the generation of new Ni species. Since the binding energy of NiO 2p 3/2 is centered at 854.4 eV, it is not feasible for the new Ni species to be identified as oxidized Ni species. An et al. [36] reported that the Ni 2p 3/2 peak of heat treated Ni_3C nanoparticles on carbon was shifted to high binding energy side (853 eV), which is in good agreement with our findings. Moreover, the appearance of more satellite peaks indicates that both metallic Ni and Ni_3C present in the used catalysts.

Fig. 11 shows the XPS spectra of Cr 2p over both the reduced and used Cr&Ni/char. No obvious difference in spectra between the reduced and used Cr&Ni/char catalyst could be found. Two remarkable peaks centered at 577.3 eV and 587.1 eV respectively, are attributed to Cr 2p 3/2 and its satellite, indicating the presence of trivalent Cr cation.

Díaz et al. studied CO_2 reforming of CH_4 reaction catalyzed by a bimetallic (Ni and Ca) catalyst supported by activated carbon. Ni_3C, identified as the active species, was also found in

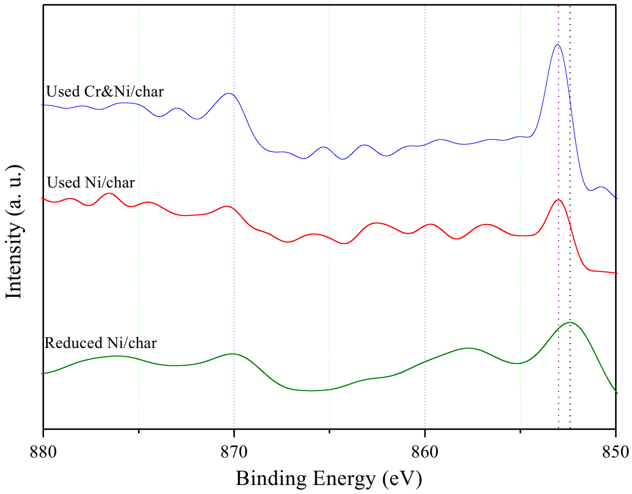

Fig. 10 – **The XPS spectra in the Ni 2p region of the reduced Ni/char, the used Ni/char, and the used Cr&Ni/char. [Reduced conditions: 600 °C, 20 ml/min H_2, 1 h; Reaction conditions: 850 °C, 8 h, Feed flow rate of 20 ml/min, $CH_4/CO_2 = 1$; Ni loading: 5 wt%; Cr loading: 7.8 wt‰.]**

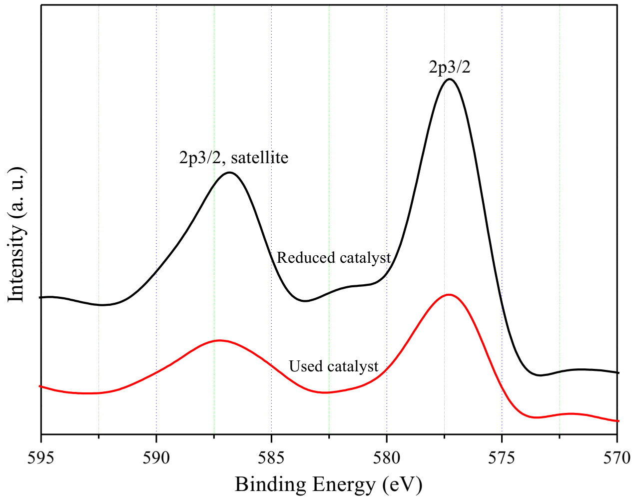

Fig. 11 – **The XPS spectra in the Cr 2p region of the reduced and used Cr&Ni/char. [Reduced conditions: 600 °C, 20 ml/min H_2, 1 h; Reaction conditions: 850 °C, 8 h, Feed flow rate of 20 ml/min, $CH_4/CO_2 = 1$; Ni loading: 5 wt%; Cr loading: 7.8 wt‰.]**

the used catalyst [37]. Transition metal carbides which possess similar chemical properties as noble metals are widely applied in various reactions, such as CH_4 reforming [38,39], hydrotreating of oil fractions [40,41], hydrodeoxygenation reactions [42–44], hydrogenation of carbon oxides, and F–T synthesis [45–47], etc. Guo et al. [39] investigated a catalyst comprising of metallic Ni and Mo_2C for CO_2 reforming of CH_4 reaction and the composite catalyst exhibits good activity and stability. In general, metal carbides can be prepared through temperature programmed process by exposing metal oxides to a gas flow of CH_4 and H_2; Zhang et al. [38] found that Ni–Mo_2C catalyst for CH_4–CO_2 reforming was in situ synthesized from $NiMoO_x$ in a feed ratio of CH_4/CO_2 equal to unity. In our study, Ni_3C was also formed in situ over char supported Ni-based catalyst during the reaction, especially after 15 min TOS. For non-carbonaceous materials supported catalysts, carbide species was also observed and recognized as an active intermediate in the reforming reaction [35,48,49].

Fig. 12 shows the H_2-TPR profiles of fresh Ni/char and Cr&Ni/char catalysts. As Fig. 12 depicts, negligible difference could be observed between the profiles of both catalysts with respect of peak position and area. Two distinct peaks centered roughly at 405 °C and 515 °C could be ascribed to the reduction of NiO with low and high interaction with the support, respectively [50]. It is widely reported that Cr could play a role in either stabilizing the material [51], while some other literature propose that Cr might be able to shift the lower reduction temperature downward [52,53]. In our study, the introduction of Cr to Ni/char catalyst does not seem to exhibit great impact on the reduction temperature.

The CO_2-TPD results of the reduced catalysts are presented in Fig. 13. It is observed that the introduction of Cr significantly enhances the adsorptive capacity of catalyst to CO_2. For the reduced catalyst without Cr, two strong CO_2 desorption peaks

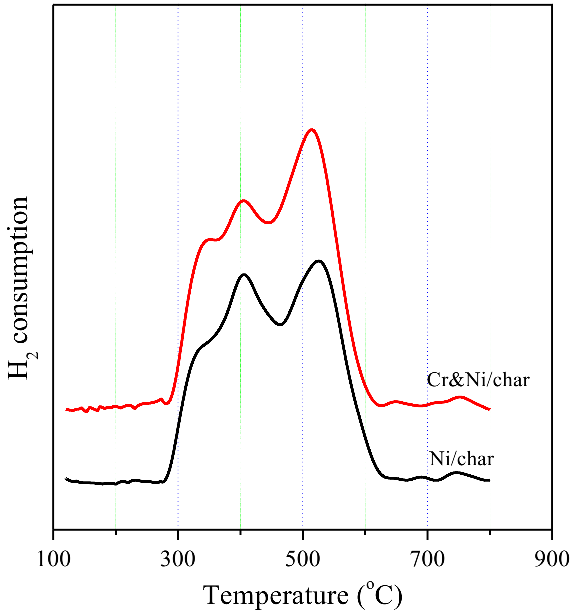

Fig. 12 – **The H_2-TPR profiles of the fresh catalysts. [Ni loading: 5 wt%; Cr loading: 7.8 wt‰.]**

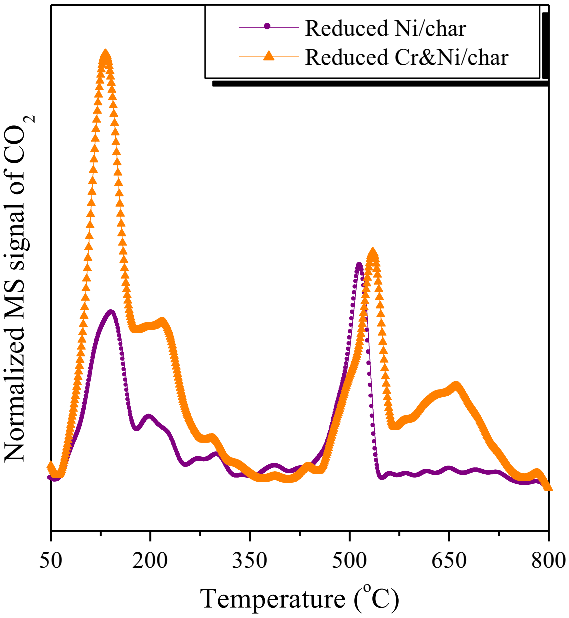

Fig. 13 – **The CO_2-TPD profiles of the reduced catalysts. [Reduced conditions: 600 °C, 20 ml/min H_2, 1 h; Ni loading: 5 wt%; Cr loading: 7.8 wt‰.]**

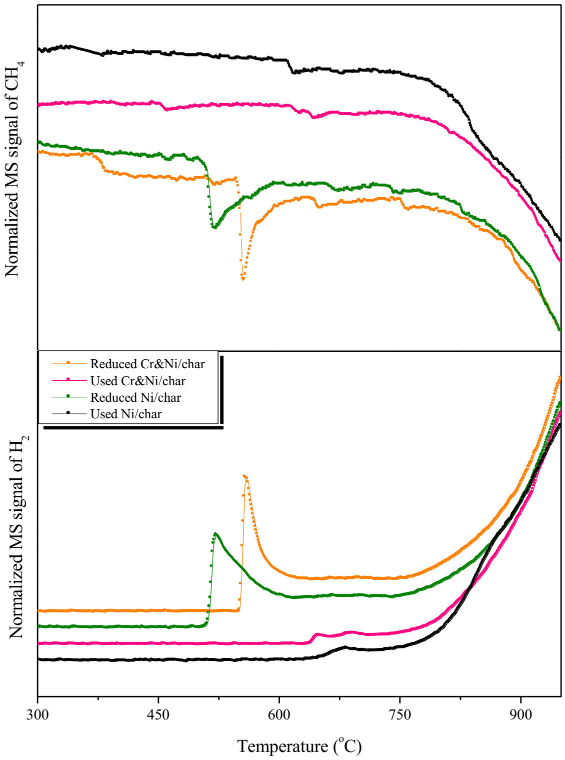

Fig. 14 – **The CH_4-TPSR profiles of the reduced and the used catalysts. [Reduced conditions: 600 °C, 20 ml/min H_2, 1 h; Reaction conditions: 850 °C, 8 h, Feed flow rate of 20 ml/min, CH_4/CO_2 = 1; Ni loading: 5 wt%; Cr loading: 7.8 wt‰.]**

positioned at about 145 °C and 515 °C as well as several weak peaks are observed. For Cr-promoted catalyst after H_2 reduction, the intensity of CO_2 desorption in the range of 50 °C–255 °C gets increased dramatically, accompanied by the appearance of another obvious CO_2 desorption peak at about 650 °C. The CO_2-TPD results indicate that the Cr-promoted catalyst has stronger affinity toward CO_2 than the catalyst without Cr addition, thereby exhibits high activity and resistance to carbon formation, which is consistent with Kim et al.'s findings [33].

Fig. 14 shows the CH_4-TPSR profiles of the reduced and used catalysts. For the reduced Ni/char catalyst, the remarkable CH_4 decomposition peak and the synchronously corresponding H_2 production peak are at about 520 °C. Several weak peaks are also detected below 800 °C, which could be assigned to different kinds of CH_x species derived from CH_4 decomposition according to reference [54–57]. For the reduced catalyst with Cr addition, both the CH_4 decomposition and the corresponding H_2 production peaks are shifted to higher temperature at about 560 °C. In the case of used catalysts, only several weak peaks (at about 650 °C and 690 °C) below 800 °C are observed. The significant difference between reduced and used catalysts lies in the amount of H_2 formed via CH_4 decomposition, which is intimately related to the carbon resistance ability of catalyst. Upon the previous discussion, Ni_3C and Ni are then confirmed to be the main active species over used and reduced catalyst, respectively. Besides, Ni_3C has a much higher resistance to coke than Ni.

Fig. 15 shows the CO_2-TPO profiles of used catalysts. According to Fig. 15, three types of deposited carbon species are found over both catalysts with and without Cr. All the carbon species can be gasified with CO_2 and the corresponding peaks are located at about 660 °C, 780 °C and 920 °C. Upon Cr addition, the peak at about 920 °C gets declined with respect to the peak area, indicating a significant reduction by 52.4% in the amount of carbon formed on the catalyst surface.

By integrate the results of catalyst characterization and catalytic performance, it is believed that Ni_3C as the main active species is formed during the reforming process. A reaction mechanism and the formation routes of Ni_3C are proposed as follows: (i) in the initial reaction period, within 15 min TOS, Ni presents to be the only active species. The reactivity of catalyst tends to decrease rapidly due to the increase of Ni particle size and carbon deposition onto the char with limited specific surface area [20]; (ii) as the reaction proceeds, the preliminary formation of Ni_3C is from the interaction between the deposited carbon and Ni under a proper molar ratio of CH_4 to H_2; (iii) The results of cyclic tests suggest that Ni_3C could be regenerated via a reduction–oxidation cycle. In these regards, the mechanism could be represented as below;

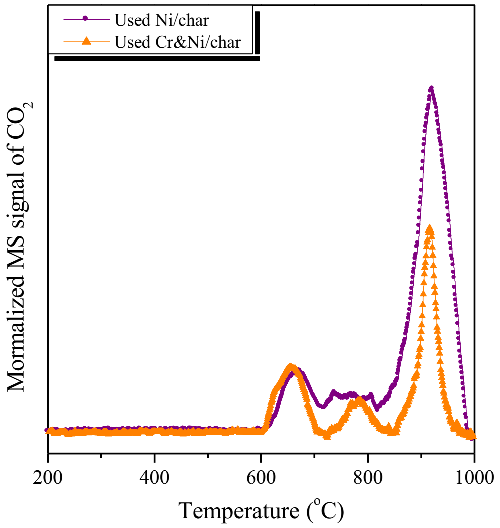

Fig. 15 – The CO_2-TPO profiles of the used catalysts. [Reaction conditions: 850 °C, 8 h, Feed flow rate of 20 ml/min, $CH_4/CO_2 = 1$; Ni loading: 5 wt%; Cr loading: 7.8 wt‰.]

$$Ni_3C + 4CO_2 = 3NiO + 5CO \tag{R2}$$

$$3NiO + 4CH_4 = Ni_3C + 3CO + 8H_2 \tag{R3}$$

It is supposed that the interaction between the carbon atom of Ni_3C and the O* originating from the dissociation of adsorbed CO_2 could generate a vacancy, making the Ni_3C more vulnerable to be oxidized. The filling of the vacancy with a C* is hence desirable to avoid bulk oxidation. In another word, if the rate of CH_4 decomposition is lower than that of CO_2 dissociation, the catalyst would more likely be oxidized and subsequently lose its activity [37]. This assumption could be demonstrated by the catalytic behavior of the cyclic tests. As the used catalyst after the first cycle was collected, the inevitable contact with air can cause the oxidization of Ni_3C. In the second cycle, the initial conversion is not as high as the final conversion of the first one. Fortunately, sustainable catalytic activity in beneficial to the recovery of Ni_3C from the following cycles proves the promising application of this catalyst in CO_2 reforming of CH_4 reaction. Moreover, two pathways can be inferred for the formation of Ni_3C: (i) the direct interaction between the deposited carbon and Ni particles; (ii) the interaction of NiO with CH_4. The second route can be considered an effective shortcut for the preparation of such catalysts with Ni_3C as the active species, avoiding unnecessary H_2 treatment.

Conclusions

The catalytic CO_2 reforming of CH_4 was studied over Cr-promoted Ni/char. The catalysts prepared by co-impregnation exhibits better activity than those prepared by sequential impregnation. An optimal Cr loading was determined as 7.8 wt‰ over 5 wt% Ni/char, which could improve the dispersion of Ni and the affinity to CO_2. It is interesting that the conversions of CH_4 and CO_2 over both Cr&Ni/char and Ni/char catalysts have an inflection point, before which the conversions rapidly decrease and after which the conversions rise up until a maximum is reached. The mechanism behind this phenomenon is revealed: Ni presents to be the major active species at the beginning of this reaction; Ni_3C formed in situ during the reforming reaction by the interaction between Ni and the deposited carbon turns out to be the new major active species. Although it is proved in this research that Ni_3C exhibits higher reactivity and stability than Ni, more in-depth investigation should be done to optimize the catalyst preparation while avoiding unnecessary reduction procedures.

Acknowledgments

The authors gratefully acknowledge financial support from National Natural Science Foundation of China (No. 21106113), China Scholarship Council (No. 201206975013), Shaanxi Province Science and Technology Research and Development of China (No. 2010K01-082),Natural Science Foundation of Shaanxi Province of China (2011JY006), and Xi'an Engineering Laboratory Project. The authors also appreciate the supports provided by the School of Energy Resources and the Department of Chemical and Petroleum Engineering at University of Wyoming for the study.

REFERENCES

[1] Kathiraser Y, Wang Z, Kawi S. Oxidative CO_2 reforming of methane in $La_{0.6}Sr_{0.4}Co_{0.8}Ga_{0.2}O_3$-delta (LSCG) hollow fiber membrane reactor. Environ Sci Technol 2013;47:14510–7.

[2] Xu L, Liu Y, Li Y, Lin Z, Ma X, Zhang Y, et al. Catalytic CH_4 reforming with CO_2 over activated carbon based catalysts. Appl Catal A Gen 2014;469:387–97.

[3] Rahemi N, Haghighi M, Babaluo AA, Jafari MF, Khorram S. Non-thermal plasma assisted synthesis and physicochemical characterizations of Co and Cu doped Ni/Al_2O_3 nanocatalysts used for dry reforming of methane. Int J Hydrogen Energy 2013;38:16048–61.

[4] Cui S, Cheng W, Shen X, Fan M, Russell A, Wu Z, et al. Mesoporous amine-modified SiO_2 aerogel: a potential CO_2 sorbent. Energy Environ Sci 2011;4:2070–4.

[5] Dutcher B, Fan M, Leonard BM, Dyar DM, Tang J, Speicher EA, et al. Use of nanoporous FeOOH as a catalytic support for $NaHCO_3$ decomposition aimed at reduction of energy requirement of Na_2CO_3/$NaHCO_3$ based CO_2 separation technology. J Phys Chem C 2011;115:15532–44.

[6] Barrai F, Jackson T, Whitmore N, Castaldi MJ. The role of carbon deposition on precious metal catalyst activity during dry reforming of biogas. Catal Today 2007;129:391–6.

[7] Ghelamallah M, Granger P. Impact of barium and lanthanum incorporation to supported Pt and Rh on alpha-Al_2O_3 in the dry reforming of methane. Fuel 2012;97:269–76.

[8] Rui Z, Fang D, Chen H, Ji H. Evaluation of TiO_2 nanotube supported Ru catalyst for syngas production. Catal Today 2013;216:178–84.

[9] Wisniewski M, Boreave A, Gelin P. Catalytic CO_2 reforming of methane over Ir/$Ce_{0.9}Gd_{0.1}O_{2-x}$. Catal Commun 2005;6:596–600.

[10] Vafaeian Y, Haghighi M, Aghamohammadi S. Ultrasound assisted dispersion of different amount of Ni over ZSM-5 used as nanostructured catalyst for hydrogen production via CO_2 reforming of methane. Energy Convers Manag 2013;76:1093–103.

[11] Liu H, Li Y, Wu H, Miyake T, He DH. CO_2 reforming of methane over Ni/SBA-15 prepared with beta-cyclodextrin: role of beta-cyclodextrin in Ni dispersion and performance. Int J Hydrogen Energy 2013;38:15200–9.

[12] Zuo ZJ, Shen CF, Tan PJ, Huang W. Ni based on dual-support Mg-Al mixed oxides and SBA-15 catalysts for dry reforming of methane. Catal Commun 2013;41:132–5.

[13] Han YK, Ahn CI, Bae JW, Kim AR, Han GY. Effects of carbon formation on catalytic performance for CO_2 reforming with methane on Ni/Al_2O_3 catalyst: comparison of fixed-bed with fluidized-bed reactors. Ind Eng Chem Res 2013;52:13288–96.

[14] Damyanova S, Pawelec B, Arishtirova K, Fierro JLG. Ni-based catalysts for reforming of methane with CO_2. Int J Hydrogen Energy 2012;37:15966–75.

[15] Kim DH, Sim JK, Lee J, Seo HO, Jeong MG, Kim YD, et al. Carbon dioxide reforming of methane over mesoporous Ni/SiO_2. Fuel 2013;112:111–6.

[16] Chen QJ, Zhang J, Jin QW, Pan BR, Kong WB, Zhao TJ, et al. Effect of reflux digestion treatment on the catalytic performance of Ni-CaO-ZrO_2 nanocomposite catalysts for CO_2 reforming of CH_4. Catal Today 2013;215:251–9.

[17] Yang EH, Kim SW, Ahn BS, Moon DJ. Preparation and characterization of Ni-based perovskite catalyst for steam CO_2 reforming of methane. J Nanosci Nanotechnol 2013;13:4334–7.

[18] Frontera P, Macario A, Aloise A, Crea F, Antonucci PL, Nagy JB, et al. Catalytic dry-reforming on Ni-zeolite supported catalyst. Catal Today 2012;179:52–60.

[19] Luengnaruemitchai A, Kaengsilalai A. Activity of different zeolite-supported Ni catalysts for methane reforming with carbon dioxide. Chem Eng J 2008;144:96–102.

[20] Guo F, Zhang Y, Zhang G, Zhao H. Syngas production by carbon dioxide reforming of methane over different semi-cokes. J Power Sources 2013;231:82–90.

[21] Dong Y, Feng M, Zhang Y, Zhao W, Cao H. CO_2 reforming of CH_4 in coke oven gas to syngas over coal char catalyst. Chem Eng J 2010;156:519–23.

[22] Cheng H, Zhang Y, Zhang G, Song S. Experimental research and numerical simulation of coal char-catalyzed CO_2 reforming of CH_4. Chem-Asian J 2013;25:3179–86.

[23] Makeswari M, Santhi T. Optimization of preparation of activated carbon from *Ricinus communis* leaves by microwave-assisted zinc chloride chemical activation: competitive adsorption of Ni^{2+} ions from aqueous solution. J Chem 2013;2013:1–12.

[24] Oezkara-Aydinoglu S, Oezensoy E, Aksoylu AE. The effect of impregnation strategy on methane dry reforming activity of Ce promoted Pt/ZrO_2. Int J Hydrogen Energy 2009;34:9711–22.

[25] Koo KY, Roh HS, Jung UH, Yoon WL. Combined H_2O and CO_2 reforming of CH_4 over Ce-promoted Ni/Al_2O_3 catalyst for gas to liquid (GTL) process: enhancement of Ni-CeO_2 interaction. Catal Today 2012;185:126–30.

[26] Yoshida K, Okumura K, Miyao T, Naito S, Ito S, Kunimori K, et al. Oxidative steam reforming of methane over Ni/a-Al_2O_3 modified with trace Pd. Appl Catal A Gen 2008;351:217–25.

[27] Kim DH, Woo SI, Lee JM, Yang OB. The role of lanthanum oxide on Pd only three way catalysts prepared by co-impregnation and sequential impregnation methods. Catal Lett 2000;70:35–41.

[28] Garcia T, Weng WH, Solsona B, Carter E, Carley AF, Kiely CJ, et al. The significance of the order of impregnation on the activity of vanadia promoted palladium-alumina catalysts for propane total oxidation. Catal Sci Technol 2011;1:1367–75.

[29] Nagaoka K, Abe Y, Hashimoto Y, Ishikawa T, Sato K, Takita Y, et al. Cr^{3+}–$Co_{0.054}Ni_{0.018}Mg_{0.93}O$ solid-solution catalysts for high-pressure syngas production: effect of chromium on the reduction and catalysis. ACS Catal 2013;3:1564–72.

[30] Xu C, Hamilton S, Ghosh M. Hydro-treatment of Athabasca vacuum tower bottoms in supercritical toluene with microporous activated carbons and metal-carbon composite. Fuel 2009;88:2097–105.

[31] Sun N, Wen X, Wang F, Wei W, Sun Y. Effect of pore structure on Ni catalyst for CO_2 reforming of CH_4. Energy Environ Sci 2010;3:366–9.

[32] Ashok J, Raju G, Reddy PS, Subrahmanyam M, Venugopal A. Catalytic decomposition of CH_4 over $NiO-Al_2O_3-SiO_2$ catalysts: influence of catalyst preparation conditions on the production of H_2. Int J Hydrogen Energy 2008;33:4809–18.
[33] Kim YT, Um JH, Kim SH, Lim TH, Lee HI. Effect of promoter on Ni/MgO catalyst in C_8H_{18} auto thermal reforming in solid oxide fuel cell system. Appl Catal A Gen 2010;384:10–7.
[34] Goto Y, Taniguchi K, Omata T, Otsuka-Yao-Matsuo S, Ohashi N, Ueda S, et al. Formation of Ni_3C nanocrystals by thermolysis of nickel acetylacetonate in oleylamine: characterization using hard X-ray photoelectron spectroscopy. Chem Mater 2008;20:4156–60.
[35] Kroll VCH, Delichure P, Mirodatos C. Methane reforming reaction with carbon dioxide over a Ni/SiO_2 catalyst: the nature of the active phase. Kinet Catal 1996;37:749–57.
[36] An C, Nakaya M, Kanie K, Muramatsu A. Synthesis of nickel compound nanoparticles on carbon and their oxygen reduction reaction. In: 5th International symposium on functional materials, December 17–20, 2012, Perth, Western Australia; 2012.
[37] Díaz K, García V, Matos J. Activated carbon supported Ni–Ca: influence of reaction parameters on activity and stability of catalyst on methane reformation. Fuel 2007;86:1337–44.
[38] Zhang A, Zhu A, Chen B, Zhang S, Au C, Shi C. In-situ synthesis of nickel modified molybdenum carbide catalyst for dry reforming of methane. Catal Commun 2011;2:803–7.
[39] Guo J, Zhang A, Zhu A, Xu Y, Au CT, Shi C. A carbide catalyst effective for the dry reforming of methane at atmospheric pressure. In: Advances in CO_2 conversion and utilization. ACS symposium series. Washington, DC: American Chemical Society; 2010.
[40] Aegerter PA, Quigley WWC, Simpson GJ, Ziegler DD, Logan JW, McCrea KR, et al. Thiophene hydrodesulfurization over alumina-supported molybdenum carbide and nitride catalysts: adsorption sites, catalytic activities, and nature of the active surface. J Catal 1996;164:109–21.
[41] Villasana Y, Escalante Y, Nunez JER, Mendez FJ, Ramirez S, Luis-Luis MA, et al. Maya crude oil hydrotreating reaction in a batch reactor using alumina-supported NiMo carbide and nitride as catalysts. Catal Today 2014;220:318–26.
[42] Boullosa-Eiras S, Lodeng R, Bergem H, Stocker M, Hannevold L, Blekkana EA. Catalytic hydrodeoxygenation (HDO) of phenol over supported molybdenum carbide, nitride, phosphide and oxide catalysts. Catal Today 2014;223:44–53.
[43] Hollak SAW, Gosselink RW, van Es DS, Bitter JH. Comparison of tungsten and molybdenum carbide catalysts for the hydrodeoxygenation of oleic acid. ACS Catal 2013;3:2837–44.
[44] Jongerius AL, Gosselink RW, Dijkstra J, Bitter JH, Bruijnincx PCA, Weckhuysen BM. Carbon nanofiber supported transition-metal carbide catalysts for the hydrodeoxygenation of guaiacol. ChemCatChem 2013;5:2964–72.
[45] Kwak G, Woo MH, Kang SC, Park HG, Lee YJ, Jun KW, et al. In situ monitoring during the transition of cobalt carbide to metal state and its application as Fischer-Tropsch catalyst in slurry phase. J Catal 2013;307:27–36.
[46] Vo DVN, Arcotumapathy V, Abdullah B, Adesina AA. Non-linear ASF product distribution over alkaline-earth promoted molybdenum carbide catalysts for hydrocarbon synthesis. Catal Today 2013;214:42–9.
[47] Wu QX, Christensen JM, Chiarello GL, Duchstein LDL, Wagner JB, Temel B, et al. Supported molybdenum carbide for higher alcohol synthesis from syngas. Catal Today 2013;215:162–8.
[48] Chen J, Wang R, Zhang J, He F, Han S. Effects of preparation methods on properties of $Ni/CeO_2-Al_2O_3$ catalysts for methane reforming with carbon dioxide. J Mol Catal A Chem 2005;235:302–10.
[49] Kroll VCH, Swaan HM, Mirodatos C. Methane reforming reaction with carbon dioxide over Ni/SiO_2 catalyst I. Deactivation studies. J Catal 1996;161:409–22.
[50] Izquierdoa U, Barrioa VL, Bizkarraa K, Gutierrezb AM, Arraibib JR, Gartziac L, et al. Ni and Rh single bond Ni catalysts supported on zeolites L for hydrogen and syngas production by biogas reforming processes. Chem Eng J 2014;238:178–88.
[51] Martos C, Dufour A. Synthesis of Fe_3O_4-based catalysts for the high-temperature water gas shift reaction. Int J Hydrogen Energy 2009;34:4475–81.
[52] Lohitharn N, Goodwin Jr JG, Lotero E. Fe-based Fischer-Tropsch synthesis catalysts containing carbide-forming transition metal promoters. J Catal 2008;255:104–13.
[53] Lohitharn N, Goodwin Jr JG. Impact of Cr, Mn and Zr addition on Fe Fischer-Tropsch synthesis catalysis: investigation at the active site level using SSITKA. J Catal 2008;257:142–51.
[54] Gao J, Hou Z, Guo J, Zhu Y, Zheng X. Catalytic conversion of methane and CO_2 to synthesis gas over a La_2O_3-modified SiO_2 supported Ni catalyst in fluidized-bed reactor. Catal Today 2008;131:278–84.
[55] Liu H, Teng B, Fan M, Wang B, Zhang Y, Harris HG. CH_4 dissociation on the perfect and defective MgO(001) supported Ni_4. Fuel 2014;123:285–92.
[56] Liu H, Wang B, Fan M, Henson N, Zhang Y, Towler BF, Harris HG. Study on carbon deposition associated with catalytic CH_4 reforming by using density functional theory. Fuel 2013;113:712–8.
[57] Triantafyllopoulos NC, Neophytides SG. Dissociative adsorption of CH_4 on NiAu/YSZ: the nature of adsorbed carbonaceous species and the inhibition of graphitic C formation. J Catal 2006;239:187–99.